AIAA SciTech Forum
8-12 January 2024, Orlando, FL
AIAA SCITECH 2024 Forum

10.2514/6.2024-2162

Thermite-for-Demise Concept: from Material Selection to Test Campaign

A. Finazzi[1], S. Carlotti[2] , C. Paravan[3], F. Maggi[4]
Politecnico di Milano, Milano, MI, 20156, Italy

S. Dossi[5]
ReActive - Powder Technology s.r.l., Milano, MI, 20123, Italy

T. Lips[6]
Hyperschall Technologie Göttingen GmbH, Bovenden, 37120, Germany

D. Daub[7], T. Schleutker[7]
Deutsches Zentrum für Luft- und Raumfahrt e.V. (DLR), 51147 Köln, Germany

G. Smet[8], K. Bodjona[8]
ESA/ESTEC, 2200 AG, Noordwijk, The Netherlands

In the frame of the ESA-TRP SPADEXO project, the use of thermites to aid spacecraft demise during re-entry is under investigation. The charges are expected to ignite spontaneously during the reentry phase, supplying additional heat to components critical for the on-ground casualty risk. This concept was explored experimentally in DLR-Cologne's L2K facility, where steel mock-ups filled with the energetic material were exposed to relevant conditions for the final application. In this paper, the selection of the pyrotechnic material will be discussed, as well as the macroscopic results obtained during the experimental campaign for one out of the three geometries explored during the project. XRD and tomography were then used to characterize the slag produced during the tests, and to explain the reasons of the unexpected pressure build-up observed during the tests involving a fraction of activated thermite.

I. Nomenclature

H_0 = Enthalpy at the standard state
M^1, M^2 = Metal elements
t = Time

[1] PhD student, Dept. Aerospace Science and Technology.
[2] Assistant Professor, Dept. Aerospace Science and Technology, AIAA Senior Member.
[3] Assistant Professor, Dept. Aerospace Science and Technology.
[4] Associate Professor, Dept. Aerospace Science and Technology, AIAA Senior Member.
[5] Chief Executive Officer.
[6] Managing Director.
[7] Research Scientist, Institute of Aerodynamics and Flow Technology, Supersonic and Hypersonic Technologies Department.
[8] Mechanisms Engineer.

T_c = Adiabatic combustion temperature
x_i = stoichiometric coefficients

II. Introduction

End-of-life management of satellites is becoming of paramount importance due to the accumulation of space debris. The most critical condition is evidenced in some Low Earth Orbits (LEO), where the number density of objects has already overcome the threshold for the initiation of the chain reaction predicted by Kessler and leading to a spontaneous growth of the number of orbiting items, due to collision. Whereas the discussion on candidate remediation methods is still open [1], mitigation measures must be put in place rapidly to contain the growth of the in-orbit junk population. Even the Council of the European Union is pushing for an urgent action, calling for a reconsideration of the current mitigation measures up to more stringent limits, as highlighted by the draft conclusions of the discussion about the "Fair and sustainable use of space" [1].

The stop of new space activities is impossible to achieve. The space economy is growing at a very high pace and forecasts are predicting an incremented exploitation of the outer space for commercial purposes. Constellations are mostly driving this trend. At the same time, nanosatellite market share is expanding and is calling for new and dedicated launch services. Under these economic push, regulatory frameworks or, at least, guidelines are urged to define methods and limits for a sustainable exploitation of the space environment (representing a 2030 sustainable development goal) [2],[3],[4]. The need for a tangible solution to pollution of the lower orbits pushed the European space community (institutions and companies) to gather around the "Zero Debris Charter", a document addressing the space economy towards undertaking a sustainable growth [5].

Guidelines acknowledged by the main space agencies impose some high-level requirements for spacecraft. The 25-year-rule and the limit of on-ground casualty risk at reentry are well known guidelines and a revision is discussed or underway, internationally [6],[7]. Both ask to implement specific design choices on the mission and on the architecture of the spacecraft. A report by the European Space Agency (ESA) depicting the status of the satellite population highlights that a wide share of the satellites launched in the last decade did not comply with these regulations. In addition, some compliant satellites did not reliably accomplish the expected end-of-life process. This last aspect also puts under the spotlight the reliability of the implemented methods. It is worth underlining that the Charter stresses for an update of the approach towards constellations, suggesting for an "aggregate" risk management.

The on-ground casualty risk requirement for spacecraft refers to international standards and regulations that seek to limit the risk posed by its reentry. One commonly cited standard constrains the risk of human casualty to less than 1 in 10,000. This requirement heavily influences spacecraft design and operation. For example, a space mission may plan to perform a controlled reentry, actively reentering the satellite in a specific unpopulated area, like the Pacific Ocean. Alternatively, a spacecraft may be designed to break apart more fully during reentry in order to limit the amount of high-energy debris that can reach the Earth's surface. This latter strategy is part of the Design-for-Demise (D4D) paradigm, which focuses on designing spacecraft components in ways that promote their complete disintegration during reentry. D4D can potentially enable uncontrolled reentry as an EOL strategy, which can in some cases significantly simplify satellite architecture, and therefore mass and cost. In the frame of the CleanSpace initiative, the European Space Agency is promoting the use of the D4D engineering approach [8].

Within the big picture of the D4D approach, one of the more recent branches currently under exploration is represented by the introduction of supplementary heat, in addition to the one received during satellite reentry. This scope can be achieved by introducing additional enthalpy sources (i.e., energetic materials) inside the components and structures of the satellite. Among the possible candidates, thermites have been selected because of their high reaction temperature, high energy density, and lower risk profile with respect to other potential reactive materials [9],[10],[11]. This approach, named Thermite-for-Demise (T4D) has been the subject of an ESA-TRP project named SPAcecraft Demise during re-entry expedited using various EXOthermic reactions (SPADEXO). The project, headed by HTG and involving research teams from DLR-Cologne (Germany), Space Propulsion Laboratory of Politecnico di Milano and Reactive - Powder Technology s.r.l. (Italy), Airbus Defence and Space (Germany) has developed theoretical frameworks and tested several representative configurations in L2K arc-heated hypersonic wind tunnel trying to uncover the potential benefits as well as the possible short-stoppers of this new method.

This paper is presenting the selection and the effects of the thermites used during the final test campaign. The experiments have been conducted in relevant environment (hypersonic wind tunnel). Results on ignition demonstrate that thermites confined in a representative vessel can be reliably triggered by the external convective heat load with a high degree of reproducibility. The paper will be closed by some considerations stemming from the experimental results, one among the other being represented by the high quantity of gas generation observed during the experiments.

III. T4D as a part of the Design-for-Demise approach

When an earth-orbiting spacecraft reaches the end of its life and descends back into Earth's atmosphere, the intense aerodynamic heating caused by high-speed reentry may melt or decompose (e.g., via pyrolysis) the materials from which the spacecraft is constructed, leading to their ablation. This is the mechanism that causes the spacecraft to break down, or 'demise'. It is important to note that the lack of oxygen at high altitudes prevents actual combustion of the materials, contradicting common visual representations that frequently and inaccurately portray a massive fireball.
The process of spacecraft demise and the corresponding loss of mass is gradual, implying that if a spacecraft contains sufficiently massive and heat-resistant components, it is possible that these may not fully break down during reentry. Consequently, high-energy remnants may reach the Earth's surface, posing a serious risk to human safety. To minimize this risk, the 'Design for Demise' (D4D) concept has emerged. This concept centers on designing spacecraft components in a manner that promotes their breakdown during Earth reentry. D4D methods to date have involved the use of alternative, less heat-resistant materials, reshaping of components to augment local heat fluxes, incorporating structural vulnerabilities to expedite spacecraft disintegration, controlling energetic fragments, and incorporating energetic materials within the spacecraft to maximize the heat available for disintegration. ESA has even established guidelines on how to validate the disintegration process through analysis and testing in support of D4D [12].

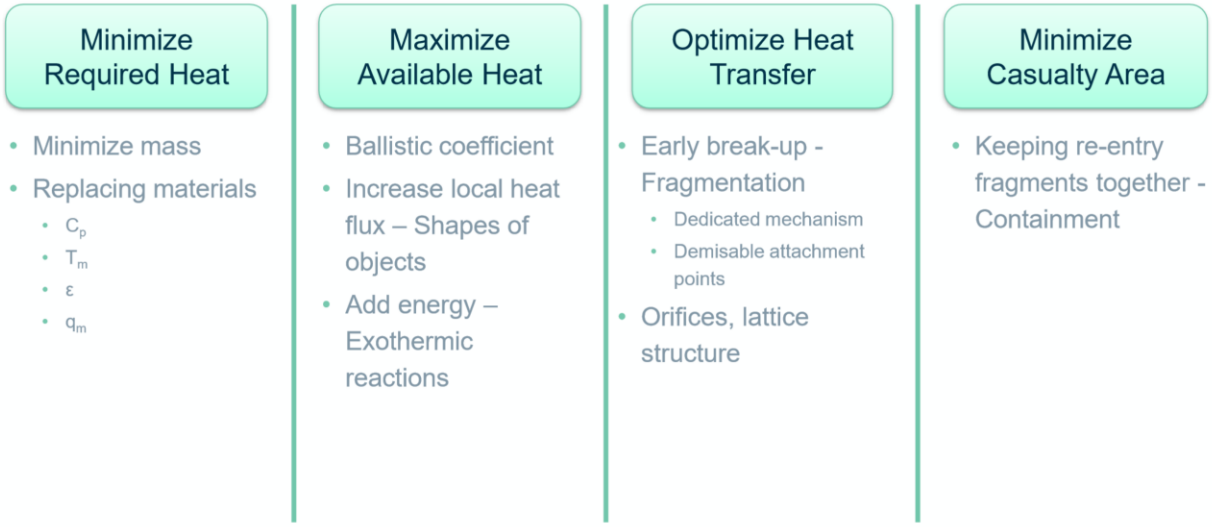

Figure 1: Strategies for Design-For-Demise

The various D4D strategies are depicted in Figure 1. At this point, there is no consensus on which strategy is best, although it is potentially feasible to combine different strategies. The present study concentrates on the second strategy illustrated, which involves maximizing the available heat during reentry. In particular, it is planned to achieve this by adding energetic material in the form of thermite to spacecraft components, a strategy we are calling Thermite-for-Demise (T4D).

IV. Thermites for satellite demise: selection criteria

The energetic materials selected for this application must comply with the fact that they take part to satellite demise activity. Powders have to accomplish both performance and programmatic requirements. Within the former category we can find the heat release, the ignition temperature, and the gas generation. In the latter one we find safety considerations, aging behavior, regulatory constraints, and similar. Some of these aspects have not yet been faced (e.g., regulatory framework, aging under space conditions).

In terms of performance behavior, a thermite is composed by a metal/metal oxide combination which undergoes redox reactions. In case of a stoichiometric reaction, the generic chemical formula written in Eq. (1) well represents the process. In there, M^1 is the starting metal oxidized by the oxygen contained in the metal oxide ($M^2_{x2}\ O_{x3}$), which eventually becomes a new metal M^2, and forming a new metal oxide ($\mathrm{M}^1_{\mathrm{x4}}\ \mathrm{O}_{\mathrm{x5}}$).

$$M^1 + \frac{x_5}{x_3\, x_4} M^2_{x2}\, O_{x3} \rightarrow \frac{1}{x_4} M^1_{x4}\, O_{x5} + \frac{x_2 x_5}{x_3\, x_4} M^2 \quad (1)$$

The spontaneity of the reaction (reduction of the Gibbs free energy) is a necessary condition. Thermodynamics dictates the enthalpy of reaction and the combustion products in ideal conditions. However, thermodynamics alone does not rule out kinetics-driven parameters, such as the rate of reaction or the ignition temperature range, and the secondary effects induced by nonideal conditions.

From the programmatic viewpoint, a thermite must be safely integrated in the spacecraft, survive for all the satellite lifetime undergoing neither ignition nor aging, and finally spontaneously react during the satellite reentry, due to aerothermal heating of the vessel. The amount of released gas depends on the intended application. If the plan is to generate a cutting torch and use it to severe parts of the spacecraft through a hot jet, a strong gas production is desired [13]. Rather, small gas generation is preferred when the intended action consists of contributing to the melting of a component embedding the powder. In the SPADEXO project, this last option was preferred. For this reason, the project focused on thermites based on iron oxide and aluminum which ideal properties are reported and compared to other aluminum-based formulations in Table 1. The aluminum - iron oxide (hematite) composition was preferred to the other thermites that were initially considered for the role of main charge thanks to its relatively high energetic density and limited gas production. Even if small amounts of more reactive thermites (e.g., Bi_2O_3) were initially considered for the role of primer, the use of mechanically activated aluminum – iron oxide thermite was then preferred due to safety reasons.

Table 1: Thermophysical properties of various Al-based thermite reactions. Data are reported per gram of reactants [14].

Oxide	$-\Delta H_0$ $[cal]$ per g of reactants	T_C, $[K]$	Gas production, $[g]$ of gas per g of products
Bi_2O_3	506.1	3253	0.8941
CuO	974.1	2843	0.3431
Fe_2O_3	945.4	3135	0.0784
Fe_3O_4	878.8	3135	0.0307
MoO_3	1124	3253	0.2473
WO_3	696.4	3253	0.1463

V. Materials and methods

1. Description of the experimental setup

The experimental campaign was performed in DLR-Cologne's arc-heated hypersonic wind tunnel L2K. It comprises a Huels-type arc-heater with a maximum electrical power of 1.4 MW. This facility can generate cold wall heat fluxes up to 3.0 MW/m^2 at stagnation pressures up to 250 hPa. A convergent-divergent nozzle produces a continuous, hypersonic gas flow that is directed on the sample. The nozzle's expansion part is conical with a half angle of 12°. The combination of different throat and nozzle exit diameters grants a high flexibility. Various test gases can be used in the wind tunnel, with the objective to replicate atmospheres typical of other planets. The reader is referred to [15] for a comprehensive description of the facility. In the SPADEXO campaign, a 29 mm nozzle throat was used in combination to a 200 mm wide exit. The working gas was air. All the tests discussed in this paper were conducted with a reference cold heat flux of 750 kW/m^2, except for Test 5, in which the heat load was increased up to 800 kW/m^2 (please refer to Table 2 for the test numbering).

2. Description of samples

Three steel sample shapes have been tested within the SPADEXO experimental campaign. The samples were in stainless steel and have been developed by the team to be representative of volume and size of a ball bearing unit (BBU) having external diameter of 50 mm and of a solar array drive mechanism (SADM). It is important to underline that the components were mockups with the sole scope to prove the T4D concept. Empty spaces were partially filled with thermite. Temperature evolution of the internal charge and of the external vessel was

accomplished by both embedded thermocouples and video recording (IR and visible range). A schematic of a thin-walled BBU and of the charge loaded in a thick-walled BBU are visible in Figure 2. A key feature of the design is the safety lid that closes the geometry on top. This layout was chosen to avoid damages to the facility in case of an excessive pressure build-up in the samples. In all the tests involving thermite that are reported in this paper, the lid was maintained in place by a couple of tungsten wires and additional venting holes were drilled in it, to assure a controlled ejection in case of an internal pressure rise. The assembled vessel was exposed to the flow of the L2K arc-heated wind tunnel (DLR-Cologne) till complete charge ignition.

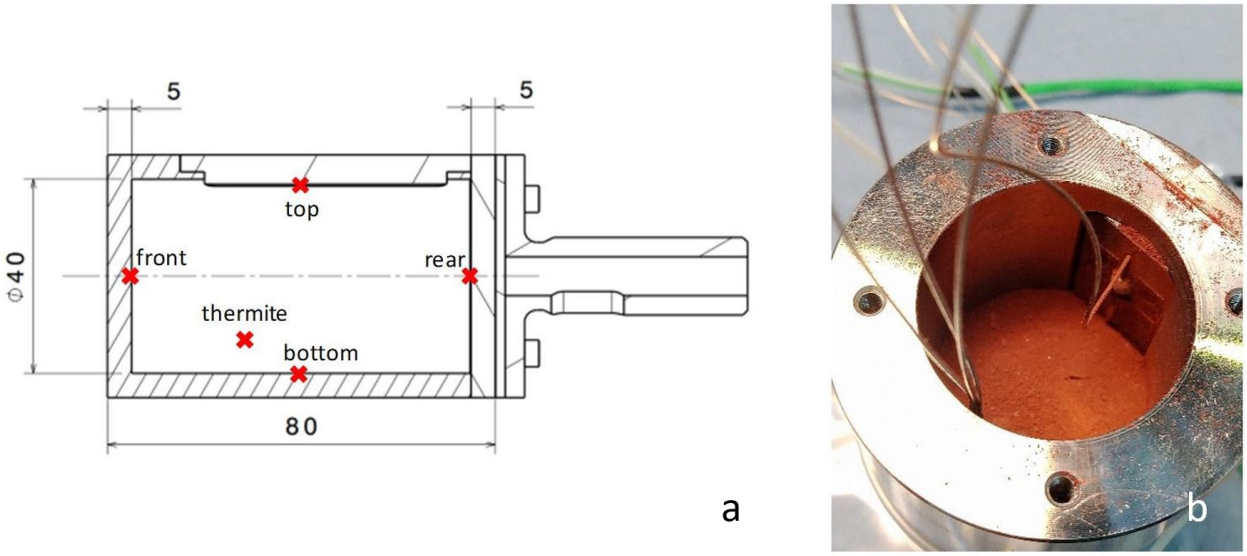

Figure 2: Ball Bearing Unit (BBU) mock-up. a) On the left, schematics with indication of thermocouple location. b) On the right, thick-walled BBU half-loaded.

In Figure 3 the reader can observe the effect of a thermite charge on one of the samples. Figure 3a reports the behavior of the vessel under wind tunnel heating, without thermite. Figure 3b is illustrating the conditions of the same item once a thermite charge ignites. The image clearly shows a strong heating contribution which eventually leads to a partial melting of the external steel vessel and loss of some molten metal drops.
Table 2 presents the thermite charge used in the tests involving the thin-walled BBU geometry. Different compositions were investigated, to experiment the effects of various fillings and activated thermite mass fractions. In Table 3 the characteristics of the starting powder are reported. The standard thermite was obtained mixing the reactants in stoichiometric ratio using a resonant acoustic mixer. The activated thermite was obtained through high-energy ball milling mechanical activation, starting from a slightly fuel-rich composition. Depending on the desired final charge, part of this mixture was shaped in the form of pellets and then dispersed in the standard thermite, while the rest was blended with the standard composition using a spoon.

3. Numerical model

A dedicated extension of the Spacecraft Atmospheric Re-entry and Aerothermal Breakup (SCARAB) was used to estimate the thermal behavior of the samples during the experimental campaign. SCARAB is an ESA tool used to predict the re-entry process of spacecraft, developed under the lead of HTG GmbH since 1995. It is one of the most prominent examples of high-fidelity re-entry models, and it is able to compute the flight dynamics, aerodynamics, aerothermodynamics, thermal and structural analysis of a re-entering spacecraft. An arbitrarily complex geometry can be represented through panelization. This software has been validated with experimental data and used successfully to simulate both real atmospheric re-entries and ground tests in wind tunnels. During the SPADEXO project, a dedicated extension has been developed to consider the effects of an internal thermite charge. The pyrotechnic material is assumed to ignite as soon as the temperature of its vessel overcomes its ignition temperature. The main effect of the thermite is a heat release that is distributed uniformly on the surface in contact with the energetic material. Please refer to [16] or [17] for further information on the numerical modeling.

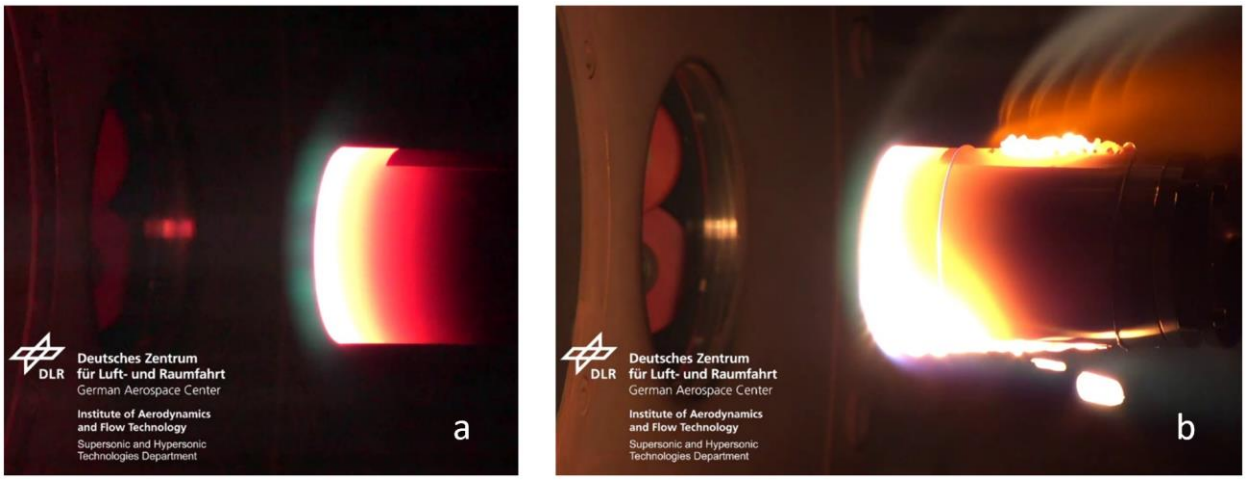

Figure 3: BBU mock-up during an arc-heated hypersonic wind tunnel experiment. a) On the left, no thermite charge. b) On the right, after ignition of internal charge.

Table 2: Subset of the tests performed during the SPADEXO experimental campaign that will be analyzed in this paper. Please note that "T" stands for standard thermite, "A" for activated loose powder, and "P" for activated pellets.

Test ID	Filling	Thermite charge [g]
1	None	-
2	26%	29.1 T
3	26%	9.2 A + 19.7 T
4	26%	9.3 P + 19.8 T
5	26%	29.1 T
6	39%	44.9 T
7	52%	58.2 T

Table 3: Characteristics of the starting powders.

Material	Characteristics
Al	Spherical, 30 μm
Fe2O3	-325 Mesh

VI. Results and discussion

1. *Macroscopic effect of the thermite charge*

At first appearance of the samples at the end of the tests was analyzed. Significant damages were observed on the front face of the sample after the tests involving thermite. Tests 6 and 7 resulted in perforation of the leading surface. Figure 4 shows the reference sample without thermite (Figure 4a) and of the one tested at the highest filling (Figure 4b) juxtaposed. Both tests were run in the wind tunnel till steady conditions were observed. Please notice that even if steady conditions for both the tests were reached after around 150 s, Test 1 was run for approximately 600 s, while Test 7 for around 300 s. This outcome proves the thermite capability to induce demise on a steel sample in relevant environment.

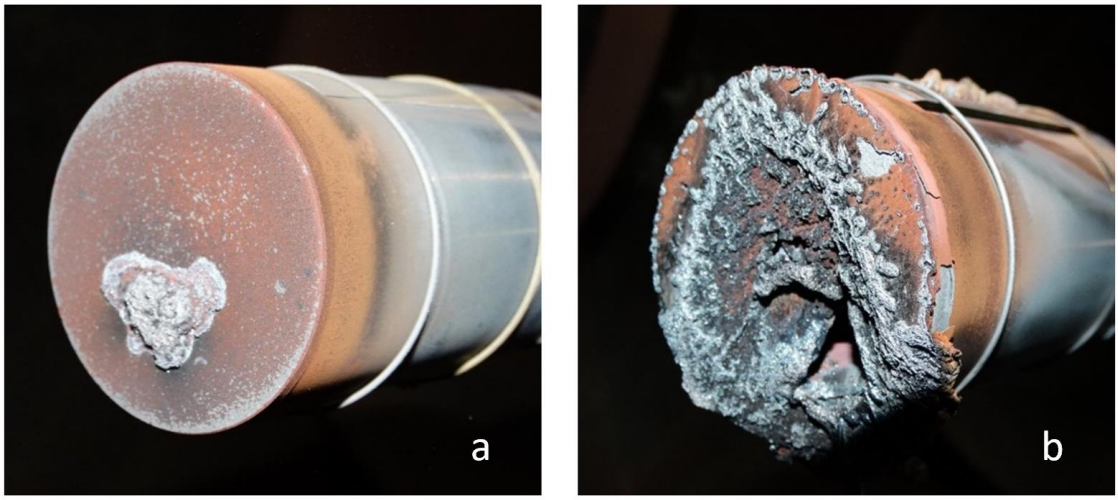

Figure 4: Appearance of the samples after the tests in the wind tunnel. a) On the left, no thermite charge (Test 1). b) On the right, with thermite charge (Test 7).

The other main result of the experimental campaign was the temperature traces registered by the thermocouples and by the pyrometers. Even if the complete dataset will be presented in further publications, the temperature increases registered by the pyrometers on the front face of the geometry are shown in Table 4. Please note that as the thermocouples were in direct contact with the pyrotechnic charge, their signal cannot be considered reliable anymore after the ignition. On the contrary, the temperature registered by the pyrometers can be used as an estimate of the (punctual) efficiency of the thermite. As the temperature trace is rather noisy, the values reported in Table 4 were determined graphically considering the instant of ignition and the instant in which the heating rate was again comparable with the one due to the sole wind tunnel heat load. Table 4 reports the temperature increase predicted by the numerical model as well. It is evident that while Tests 2 and 5 are in good agreement with the numerical model, the expected temperature increase for Tests 3 and 4 is considerably higher than the measured one. Please note that Tests 6 and 7 involved significant melting of the front face, therefore the most significant parameter of merit is the predicted demise and not the temperature increase registered on the front face. This subject is still under consideration and there is not yet a concluding position. In this paper, the reason behind the discrepancy between the experimental and the predicted temperature increase of the front face for Tests 3 and 4 will be investigated.

Table 4: Approximated temperature increase measured by the pyrometers on the front face compared with the expected one predicted by numerical simulations. Please note that P1 and P2 stand for the two different pyrometers, while the asterisk (*) indicates a simulation in which the melting of the front face is predicted.

Test ID	Total mass of thermite [g]	Temperature increase P1/P2 [K]	Expected temperature increase [K]
1	None	-	-
2	29.1	195/165	180
3	28.9	100/140	290
4	29.1	180/170	300
5	29.1	220/170	155
6	44.9	285/225	125*
7	58.2	400/245	125*

2. Thermal camera

The videos recorded by the thermal camera can help in understanding the discrepancy observed in Section VI. Figure 5 and Figure 6 report respectively six frames of Tests 2 and 3. The ignition of the powder in the samples can be determined by looking at the exhaust gases ejected by the venting holes. In Test 2 the heating of the lid is almost absent, while the fore part of the mock-up increases dramatically its temperature. Please note that it is reasonable to assume that the enthalpy released by the thermite distributed almost uniformly on the entire internal surface. This is probably the reason of the good agreement between the experimental and numerical results. On the contrary, in Test 3 it is possible to see how after the ignition of the powder the temperature of the safety lid suddenly increases. It is hereby suggested that this different behavior is due to the higher pressure build-up in the sample, that results in the ejection of a higher fraction of material. This can be verified as well by considering the weight of the system before and after the test. In Table 5 the formulation of the pyrotechnic charge and the mass loss registered for Tests 2, 3, and 4 are reported. The other tests are not considered either because no thermite was involved (Test 1) or because partial demise of the mock-up was achieved (Tests 5, 6, and 7) making impossible to distinguish between the loss of reactive material or steel. It is then evident how the presence of the activated thermite in the composition resulted in the partial loss of a relatively high fraction of the starting reactive material, up to approximately one third. Moreover, the ejection of part of the exothermic material provoked a non-uniform distribution of the reaction enthalpy on the internal surface. The area nearby the venting holes, that acted similarly to nozzles, was heated significantly. As the measure of the heat transfer efficiency provided by the pyrometers is only punctual, this parameter of merit is not appropriate to evaluate the overall energy transferred by the thermite to its vessel in the case of uneven distribution of heat on the internal surface.

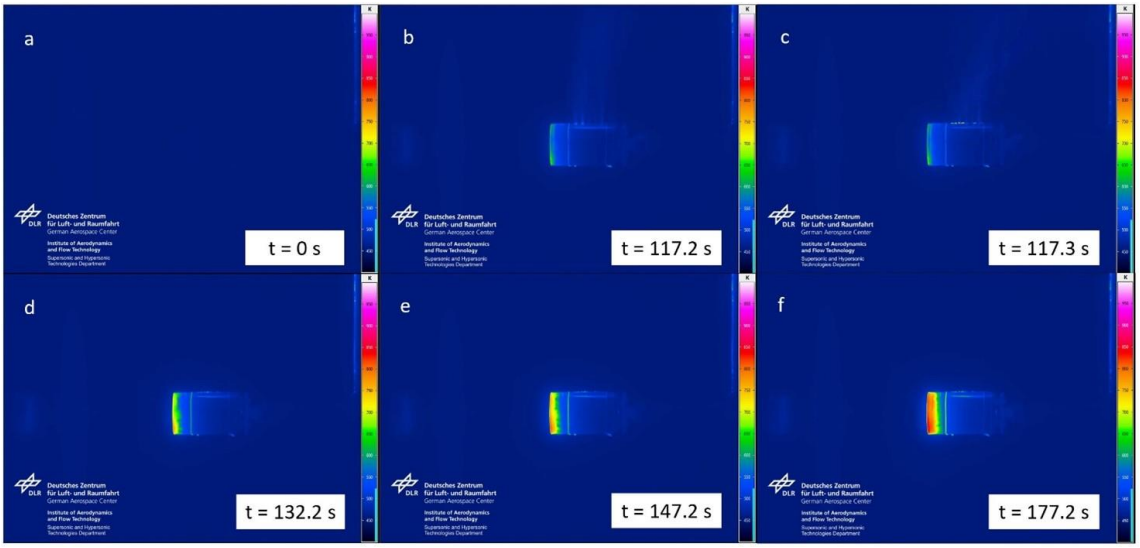

Figure 5: IR frames of Test 2, involving thin-walled BBU geometry at 26% filling, standard thermite, stagnation cold wall heat flux of 0.75 MW/m^2. a) Alignment of the sample. b) Ignition. c) Highest temperature of the lid. d) 15 s after the ignition. e) 30 s after the ignition. f) 60 s after the ignition.

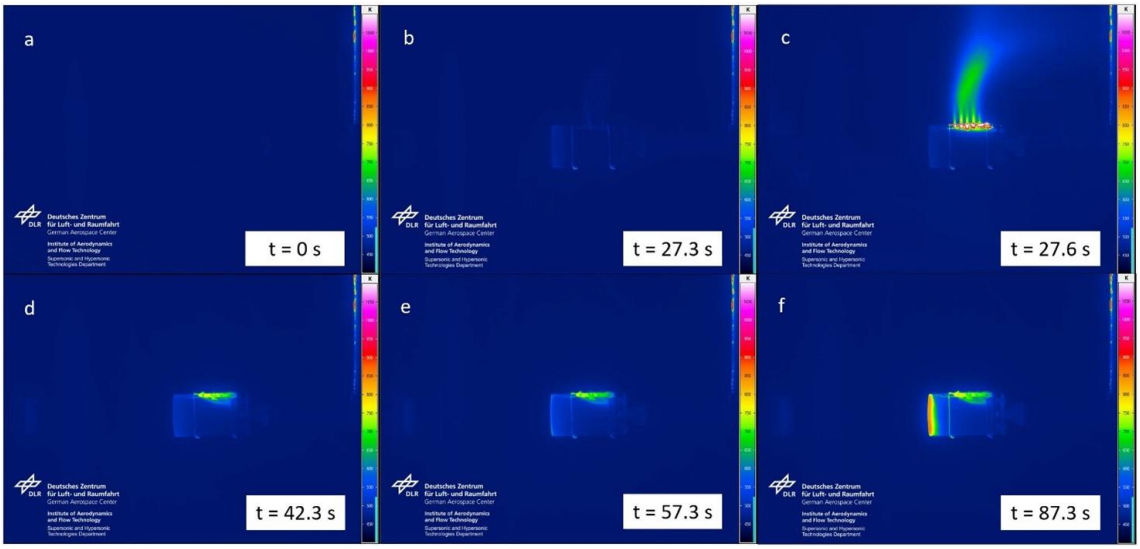

Figure 6: IR frames of Test 3, involving thin-walled BBU geometry at 26% filling, blend of standard thermite (68%) and activated loose thermite (32%), stagnation cold wall heat flux of 0.75 MW/m^2. a) Alignment of the sample. b) Ignition. c) Highest temperature of the lid. d) 15 s after the ignition. e) 30 s after the ignition. f) 60 s after the ignition.

Table 5: Thermite charge and mass loss measured after the experiments. Please note that only the tests involving thermite that did not result in the partial demise of the mock-up are considered. "T", "A", and "P" stand respectively for standard, activated loose, and activated pelletized thermite.

Test ID	Total mass of thermite [g]	Formulation	Mass loss [g]
2	29.1	100% T	-0.6
3	28.9	68% T + 32% A	-10.2
4	29.1	68% T + 32% P	-5.7

3. X-Ray Diffraction analysis

X-Ray Diffraction analysis technique was then used to gather more information about the causes of the reactive material ejection (Tests 3 and 4) and about the partial demise of the mock-ups (Tests 5, 6, and 7). In particular, the samples related to Tests 3 and 7 were selected, as these were the cases in which the highest ejection and the highest demise were experienced. Table 6 reports the results of the performed XRD analyses and the area of the mock-ups where the powder samples was scratched away. The XRD performed on the sample originating from the area nearby the venting holes of the mock-up of Test 3 shows that the resolidified material is almost totally alumina. This result is in contrast with the partial gasification of iron that should be expected for this composition if a reaction in stoichiometric condition occurs [14]. However, the crystalline species recognized suggest either or the expulsion of molten alumina, later resolidified, or the partial gasification of unreacted aluminum, with its successive oxidation once reached by the incoming air flux. The second option seems the more appropriate, considering the peculiarities of the mechanical activation process. During the activation, the aluminum powder is deformed, and part of the active metal is exposed to the contact to the iron oxide. Therefore, it is common to start from a fuel-rich composition. The amount of fuel in excess is determined empirically, aiming at a formulation that at the end of the process reaches the desired conditions (in this case, stoichiometry). Unfortunately, the active metal content of the activated powder was not checked before the experimental campaign in the wind tunnel. It is then possible that for the batch used in this set of tests the final composition was rich, determining a fuel-rich formulation. This possible excess of aluminum could explain the crystalline species obtained through XRD and, at least partially, the unexpected pressure build-up in the sample. It is necessary to remind as well that, for sure, the higher reactivity of the powder blend is a second reason of the high internal pressure.

Conversely, the XRD analyses on the mock-up subjected to Test 7 were focused on the investigation of the demise process. The material scratched from the front face of the sample was identified mainly as Fe_3O_4 (around 97%). It is suggested that this oxide was formed due to the exposure of the Fe produced by the thermite reaction to the low-pressure air flow. It is possible that during this experiment the front face of the sample was damaged up to its partial substitution with the products of the internal reaction. More results linked to this hypothesis will be presented in the next section. The XRD analysis was conducted as well on a fraction of the powder contained in the sample bag, that probably detached from it during the transportation. It is hereby assumed that this material represents an average sample of the thermite products. In this case the detected species show a distribution that is more typical of the kinetic mechanism of the aluminum – iron oxide thermite kinetic chain. More than one fifth of the sample is recognized as $FeAl_2O_4$. The diffusion of Al in this species has been previously recognized as the main process controlling the reaction [18]. The result of the XRD analysis is then coherent with this explanation, as no metal aluminum is found anymore. Lastly, the same test was performed on the resolidified material on the internal surface in the proximity of the rear of the sample. This choice was mainly driven by an unexpected pinkish color that was observed. The crystalline species recognized show a very low fraction of the initial reactants (just traces of Al^0 and less than 4% of Fe_2O_3), coherently with the other results collected for the same sample. More interestingly, a significant fraction of $MgAl_2O_4$ (11.9%) is observed. The presence of Mg can be probably explained by the layer of magnesium oxide that usually protects the thermocouple junction, as this species should not be present in the other components (pyrotechnic charge, steel 316L or thermal paste). Moreover, the spinel is probably the cause of the pinkish color observed and could have interfered with the normal kinetic chain of the thermite reaction.

Table 6: XRD analysis results, with the indication of the extraction area of the sample.

Test ID	Recognized species	Extraction
3	α-Al_2O_3 (91.1%), $FeAl_2O_4$ (6.3%), Al^0 (2.6%)	Near venting holes
7	Fe_3O_4 (96.7%), Fe_2O_3 (3.3%)	Front face
7	Fe_3O_4 (37.1%), Fe_2O_3 (7.3%), $FeAl_2O_4$ (22.6%), α-Al_2O_3 (33.0%)	Loose, unspecified location
7	Fe^0 (4.7%), Fe_2O_3 (3.7%), $FeAl_2O_4$ (29.1%), α-Al_2O_3 (50.6%), $MgAl_2O_4$ (11.9%), Al^0 (traces)	Rear internal surface

4. *Tomography*

A tomography was performed on the thin-walled BBU after Test 7 to investigate the effect of the pyrotechnic reaction on the face exposed to the incoming flow. Figure 7 shows the appearance of the front face of the sample, while Figure 8 and Figure 9 its sections obtained thanks to the tomograph. It is possible to observe the significant damages induced by the internal reactions. Noticeably, even the areas that were not perforated during the test show a decrease in thickness (from 5 mm to around 3.5 mm). From the same sample a shard was retrieved and analyzed as well with the same technique. Its color and texture closely resembled the ones that can be found in the front face of the sample. The tomography revealed that the fragment was composed of two main materials: a more porous and darker matrix in which some denser and brighter inclusions were dispersed. The reddish shade that can be observed in Figure 10a is probably due to the presence of unreacted Fe_2O_3, but it is hereby suggested that this is not one of the two materials that can be observed through the tomograph. It is evident that neither the darker matrix nor the brighter inclusions could be hematite. Instead, these materials respectively remind the colors of Fe_3O_4 and Al_2O_3. Please note that the shard is rather fragile, as well as any other material resolidified on the internal surface of the sample. All the samples were opened without effort at the end of the test campaign. Even if the thermite products have a high melting point, the result of the reaction is a fragile and porous compound. This result is considered beneficial when considering the final application of the reactive material, that is aiding spacecraft demise during re-entry.

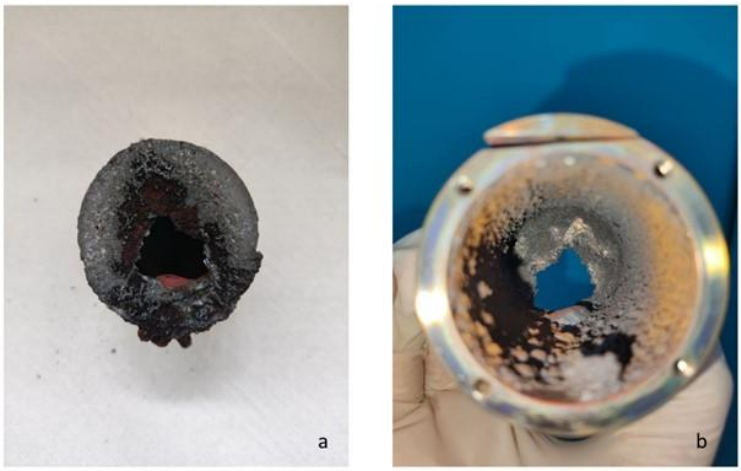

Figure 7: Final geometry of the sample after Test 7. a) Front view. b) Internal view.

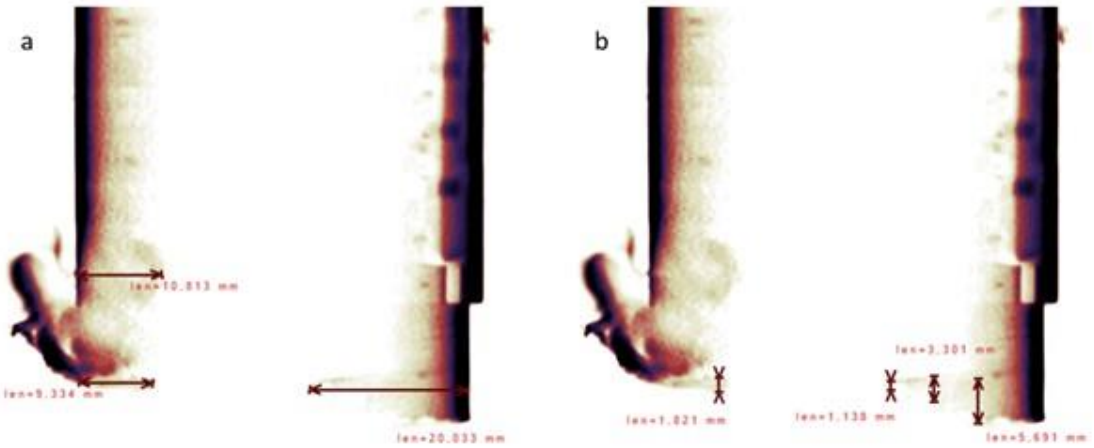

Figure 8: Section of thin-walled BBU geometry (Test 7) in the area where it is not possible to detect a continuous material. a) Horizontal thickness measures. b) Vertical thickness measures

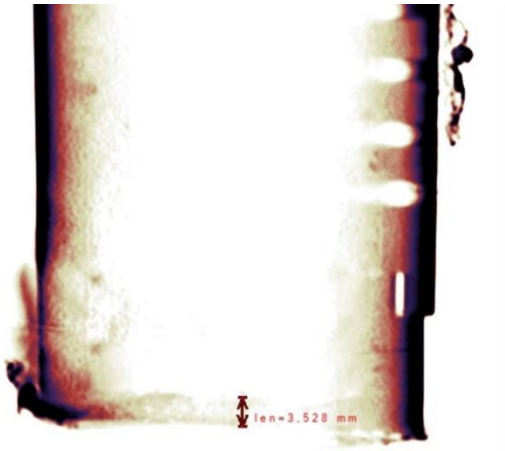

Figure 9: Section of thin-walled BBU geometry (Test 7), in the area where no hole on the front face is detected. Nevertheless, the measured thickness of the front face (3.5 mm) is lower than the one of the virgin sample (5 mm) and X-ray absorption underlines reduction of density with respect to side walls.

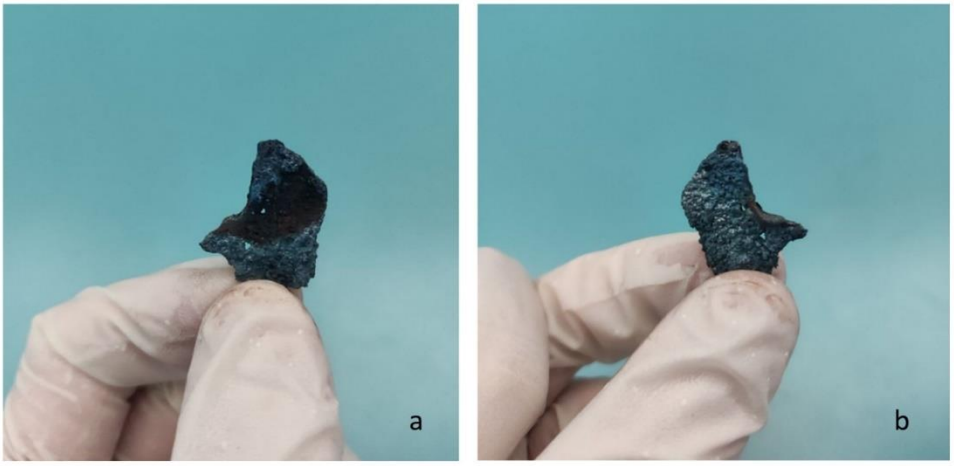

Figure 10: Fragment of thin-walled BBU (Test 7) that was analyzed using the tomograph. a) Front. b) Rear.

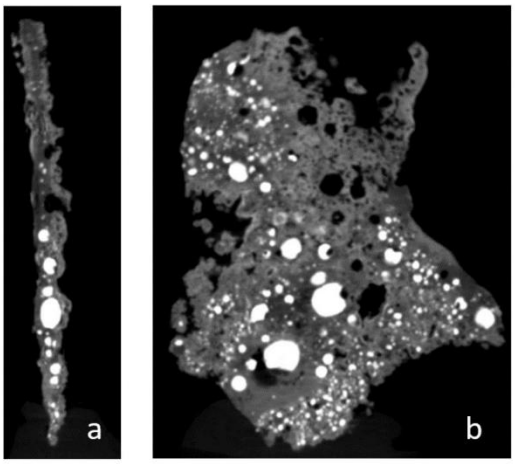

Figure 11: Tomographic sections of the thin-walled BBU shard (Test 7).

VII. Conclusion

In this paper, the selection of the energetic material for aiding spacecraft demise during re-entry has been discussed, as well as the thermite-induced demise that was observed on steel mock-ups during the experimental campaign in relevant environment. The pyrotechnic material ignited reliably in all the test runs, and successfully induced partial demise even at relatively low filling ratios. Good agreement between the numerical model and the experimental results was observed for the tests involving standard thermite. The inclusion of a significant fraction of activated thermite led to the ejection of part of the reactive material through the venting holes, that resulted into an uneven distribution of the heat load. This phenomenon was registered by the thermal camera but could not be represented properly in the current version of the software. The XRD analysis suggested that this unexpected pressure build-up was due to a fuel-rich activated thermite, coupled with the higher reactivity of the material itself. The results of the same analysis performed on the material scratched from the front face of the sample subjected to Test 7 showed that almost the totality of the surface was composed of Fe_3O_4. This indicates substantial degradation of the starting steel, or even the substitution of the starting material with the Fe produced by the internal reaction, later oxidized by the incoming air flow. The tomography performed on the same sample highlighted that the thermite products exposed to the external low-pressure air flow tend to form a porous, darker matrix (probably Fe_3O_4) in which solid, brighter inclusions (probably Al_2O_3) can be observed. This slag proved to be rather fragile. In further publications, all the results of the SPADEXO experimental campaign will be presented.

Acknowledgments

The authors acknowledge the financial support of the SPADEXO project by the European Space Agency through the Contract No. 4000136082/21/NL/MG. Tomographic scans are part of a collaboration between Space Propulsion Laboratory SPLab-POLIMI and Advanced Manufacturing Laboratory (AMALA) of Politecnico di Milano.

References

[1] Anon. Draft Council conclusions on “Fair and sustainable use of space”. Council of the European Union, May 5th, 2023.
[2] Anon., “Space Debris Mitigation Policy for Agency Projects”, ESA/ADMIN/IPOL(2014)2, ESA Director General’s Office, 2014
[3] AA.VV. “Space systems - Space debris mitigation requirements”, ISO 24113:2019, International Organization for Standardization, BSI Standards Publication.
[4] Perrault S., Soares T., and Innocenti L.. “Re-entry strategies to comply with Space Debris Mitigation guidelines”, *1st International Orbital Debris Conference*, 9-12 December 2019, Sugar Land (TX), USA.
[5] AA.VV. The Zero Debris Charter, https://www.esa.int/Space_Safety/Clean_Space/The_Zero_Debris_Charter, ESA Website, Last visited 04/12/2023.
[6] Anon. ESA’s Zero Debris approach, https://www.esa.int/Space_Safety/Clean_Space/ESA_s_Zero_Debris_approach, ESA Website, Last visited 04/12/2023.

[7] Anon. FCC Adopts New '5-Year Rule' for Deorbiting Satellites to Address Growing Risk of Orbital Debris, News Release, Federal Communications Commission, 29 sept. 2022.
[8] Cattani B.M., et al. “An Overview of design-for-demise technologies”, *8th European Conference on Space Debris*, 20-23rd April 2021, Darmstadt, Germany
[9] Dilhan, D., and Omaly, P, “Element de vehicule spatial a capacite d'autodestruction amelioree et procede de fabrication d'un tel element”, *Patent FR2975080B1*, filing year 2011.
[10] Seiler, R., and Smet, G., “Exothermic reaction aided spacecraft demise during re-entry”, *Patent EP3604143A1*, filing year 2018.
[11] Monogarov, K.A., Melnikov, I.N., Drozdov, et al. “Pyrotechnic Approach to Space Debris Destruction: From Thermal Modeling to Hypersonic Wind Tunnel Tests”. *Acta Astronautica* , Vol. 172, pp. 47-55, 2020.
[12] European Space Agency. “DIVE – Demise Verification Guidelines for Analysing and Testing the Demise of Man Made Space Objects during re-entry”, 2020.
[13] Carter, G. Jr., “Portable Metal Cutting Pyrotechnic Torch”, US Patent 2003/0145752A1, 2002.
[14] Fischer, S.H., and Grubelich, N.C., “Theoretical Energy Release of Thermites, Intermetallics, and Combustible Metals”, *24th International Pyrotechnics Seminar*, Monterey, CA. July 1998.
[15] Gülhan, A., and Esser, B., “Arc-Heated Facilities as a Tool to Study Aerothermodynamic Problems of Reentry Vehicles”, In: *Advanced Hypersonic Test Facilities*, edited by D. Marren and F. Lu, American Institute of Aeronautics and Astronautics, 2002.
[16] Finazzi, A., Maggi, F., Paravan, C., Daub, D., Dossi, S., Murgia, A., Lips, T., Smet, G., and Bodjona, K., “Thermite-for-Demise (T4D): Preliminary assessment on the effects of a thermite charge in arc-heated wind tunnel experiments”, *Aerospace Europe Conference 2023 – 10th EUCASS – 9th CEAS*, Lausanne, Switzerland, 2023.
[17] Finazzi, A., Finocchi, P., Carlotti, S., and Maggi, F., Thermite-for-Demise (T4D): Experimental analysis of heat transfer principles and preliminary sizing of an application, *International Journal of Heat and Mass Transfer*, Vol. 220, No. 124957, 2024.
[18] Fan, R., Lü, H., Sun, K., Wang, W., and Yi, X., “Kinetics of thermite reaction in Al-Fe2O3 system”, *Thermochimica Acta*, Vol. 440, pp. 129–131, 2006.